ELSEVIER

Comput. Methods Appl. Mech. Engrg. 141 (1997) 247–264

Computer methods in applied mechanics and engineering

Complex variable approach to the BEM for multiple crack problems

Mitsunori Denda *, Y.F. Dong

Rutgers University, Mechanical and Aerospace Engineering Department, P.O. Box 909, Piscataway, NJ 08855-0909, USA

Received 26 August 1994; revised 23 July 1995

Abstract

A boundary element method for straight multiple center and edge crack problems is developed in this paper. The method is constructed upon the systematic use of the elastic singularity solutions in complex variables. The crack opening is represented by the continuous distribution of dislocation dipoles and the effect of the non-crack boundary by the continuous distributions of point forces and dislocation dipoles. The crack-tip singularity is embedded into the interpolation using orthogonal polynomials (i.e. Chebyshev and Jacobi) and their associated singular weight functions. The proposed analytical integration procedure of the Cauchy-type integrals defined over the crack eliminates the need for the quadrature formulae for numerical integration, streamlines, and enhances the accuracy of the traditional singular integral equation method for crack problems. The stress intensity factors for the fifteen problems analyzed in this paper have been accurate enough to substitute those given in stress intensity factor handbooks. Since non-crack boundary of arbitrary shape can be introduced at will the method is expected to give accurate stress intensity factors for complex real life problems.

1. Introduction

The aim of this paper is to establish a numerical technique for elastic multiple crack problems that is both extraordinarily versatile and accurate. The versatility is brought in by the systematic use of elastic fundamental solutions in the formulation. The accuracy is maintained by maximizing the chance of analytical evaluation which is made possible by the use of complex variables. The fundamental solutions of elasticity, i.e. point force, dislocation, their dipoles, and the continuous distributions or layers of these singularities constitute the basic building blocks. We identify these tools and their roles in the elastic multiple crack problems, construct, and use them systematically with the help of Muskhelishvili's [1] complex variable formalism for elasticity.

Analyses of cracks in arbitrarily shaped finite bodies require numerical methods such as the boundary element method for which several excellent textbooks exist [2,3]. We develop a direct formulation of the boundary element method in complex variables based on the physical interpretation of Somigliana's identity [4,5]. The use of complex variables in the boundary element method has been more common for potential problems [6] than in elasticity problems [7] despite the rich tradition of the complex variable methods in plane elasticity [8–10]. Several crack modeling strategies by the boundary element method exist such as the multi-domain formulation [11,12], the stress formulation with regularization [13], and the dual boundary element method [14,15]. For each formulation there exist options of building in the crack tip singularity [16,17], using the quarter-point boundary element [11,18], and the strategic refining of the near crack tip elements. Further details on crack analysis, including the Green's function method [12,19], by the boundary element method are given in [20,21].

*Corresponding author.

0045-7825/97/$17.00 © 1997 Elsevier Science S.A. All rights reserved
PII S0045-7825(96)01120-6

Among numerous papers on two-dimensional multiple crack problems the majority uses Muskhelishvili's complex variable formalism. Two distinct approaches exist, one of which uses the solution on the crack surface loading [22–24] and the other the continuous distribution of dislocations [10,25,26]. The resulting system of integral equations are solved either by the special quadrature for the singular integrals [10,26], the regularization [25], the collocation [24], or the alternating method [22,23]. In this paper we model cracks by dislocations focusing attention to straight center and edge cracks. The crack opening displacement of the individual crack is modeled along the whole crack length by the continuous distribution of dislocation dipoles using the orthogonal polynomials. The resulting Cauchy-type integrals are evaluated analytically, a departure from the widely used quadrature formula approach [27–30]. No quadrature formula is used to maintain the accuracy and simplicity. This dislocation modeling scheme of cracks will be called the crack source method.

2. Elastic singularity solutions in complex variables

The singularity solutions of elasticity consist of point force, dislocation, their dipoles, and the continuous distributions or layers of these singularities. A systematic derivation of these solutions is given by the Muskhelishvili's [1] complex variable formalism for plane isotropic elasticity in which the solutions are given in terms of two analytic functions or complex potential functions, $\phi(z)$ and $\psi(z)$, of a complex variable $z = x + iy$. Cartesian vectors are represented in the complex variable form such as $u = u_x + iu_y$ and $t = t_x + it_y$ for the displacement and the traction, respectively. The displacement and the stress components are given by

$$2\mu u = 2\mu(u_x + iu_y) = \kappa\phi(z) - z\overline{\phi'(z)} - \overline{\psi(z)}, \tag{1}$$

and

$$\frac{\sigma_{xx} + \sigma_{yy}}{2} = 2\,\mathrm{Re}\,\{\phi'(z)\},$$
$$\frac{\sigma_{yy} - \sigma_{xx}}{2} + i\sigma_{xy} = \bar{z}\phi''(z) + \psi'(z), \tag{2}$$

where μ is the shear modulus and κ is given by $\kappa = 3 - 4\nu$ in plane strain and $\kappa = (3 - \nu)/(1 + \nu)$ in plane stress in terms of Poisson's ratio ν. A prime attached to the analytic functions of z indicates differentiation with respect to z and a bar indicates the complex conjugate. The symbol Re indicates the real part of the complex variable. The traction on a line segment with the slope θ is given by

$$t = t_x + it_y = -2ie^{i\theta}\,\mathrm{Re}\,\{\phi'(z)\} - ie^{-i\theta}\left\{z\overline{\phi''(z)} + \overline{\psi'(z)}\right\}. \tag{3}$$

2.1. Fundamental solutions

Consider a point force with the magnitude $f = f_x + if_y$ (per unit thickness) and an edge dislocation with the Burgers vector $b = b_x + ib_y$ located, independently, at ξ in the infinite isotropic medium. The solutions of the two problems are given in the form [31,32]

$$\phi^{(s)}(z;\xi) = -\gamma\log(z - \xi),$$
$$\psi^{(s)}(z;\xi) = -k\bar{\gamma}\log(z - \xi) + \gamma\frac{\bar{\xi}}{z - \xi}, \tag{4}$$

where

$$\begin{cases} k = -\kappa, & \gamma = f/2\pi(\kappa + 1) \quad \text{point force,} \\ k = 1, & \gamma = i\mu b/\pi(\kappa + 1) \quad \text{dislocation.} \end{cases} \tag{5}$$

When a pair of point forces $-f$ and f (or a pair of edge dislocations with the Burgers vectors $-b$ and b) are located at an infinitesimal distant $d\xi$ apart we have a force dipole (or a dislocation dipole). The force dipole represents a couple and the dislocation dipole represents a displacement discontinuity of magnitude b over the infinitesimal line segment $d\xi$. The dipole solution is obtained by applying the total differentiation operator [31,32]

$$d(\cdots) = \frac{\partial}{\partial \xi}(\cdots)\, d\xi + \frac{\partial}{\partial \bar{\xi}}(\cdots)\, d\bar{\xi}, \tag{6}$$

to the point force or the dislocation solution (4), keeping the coefficient γ constant, with the result

$$\phi^{(d)}(z;\xi) = -\gamma\, d\{\log(z-\xi)\},$$
$$\psi^{(d)}(z;\xi) = -k\bar{\gamma}\, d\{\log(z-\xi)\} + \gamma d\left\{\frac{\bar{\xi}}{z-\xi}\right\}, \tag{7}$$

where γ and k are given by (5).

2.2. Continuous distributions of singularities (layer potentials)

Introduce a smooth oriented arc L on which the position of an arbitrary point ξ is specified by an arc length parameter s. Consider the continuous distribution of the point forces (or the dislocations) over the infinitesimal line segment ds of the arc L. We define the density function $\Gamma(s)$ by γ per unit arc length, which represents the traction (or the dislocation gradient) over ds. For the continuous distribution of the point forces (or the dislocation) over the entire arc L, the complex potential functions are given by the line integral,

$$\phi^{(s)}(z) = -\int_L \Gamma(s)\log(z-\xi)\, ds,$$
$$\psi^{(s)}(z) = -k\int_L \overline{\Gamma(s)}\log(z-\xi)\, ds + \int_L \Gamma(s)\frac{\bar{\xi}}{z-\xi}\, ds. \tag{8}$$

The complex potential functions for the continuous distribution of force dipoles (or the dislocation dipoles) over L is obtained by integrating (7) directly along L with the result

$$\phi^{(d)}(z) = -\int_L \gamma(s)\, d\{\log(z-\xi)\},$$
$$\psi^{(d)}(z) = -k\int_L \overline{\gamma(s)}\, d\{\log(z-\xi)\} + \int_L \gamma(s)\, d\left\{\frac{\bar{\xi}}{z-\xi}\right\}, \tag{9}$$

where the constant k and the density function $\gamma(s)$ are specified by (5).

Mathematical methods of two-dimensional elasticity [9] are based on various integral representations of the complex potential functions such as (8) and (9) and their variations such as (10) below. The complex potential functions (8) for the continuous distribution of point forces (or edge dislocations) can also be called the single-layer potentials while those (9) for the force dipoles (or dislocation dipoles) double-layer potentials [33]. Through the integration by parts, the single-layer potentials can be transformed to the double-layer potentials (plus additional non-integral terms) and vice versa. As an example, the double-layer potential functions (9) can be rewritten as

$$\phi^{(d)}(z) = \int_L \frac{d\gamma(s)}{ds}\log(z-\xi)\, ds - [\gamma(s)\log(z-\xi)],$$
$$\psi^{(d)}(z) = k\int_L \frac{d\overline{\gamma(s)}}{ds}\log(z-\xi)\, ds - \int_L \frac{d\gamma(s)}{ds}\frac{\bar{\xi}}{z-\xi}\, ds - k\left[\overline{\gamma(s)}\log(z-\xi)\right] + \left[\gamma(s)\frac{\bar{\xi}}{z-\xi}\right], \tag{10}$$

where the integral terms are now single-layer and the non-integral terms must be retained unless $\gamma(s)$ is zero at the end points. This transformation can be used to change the order of the kernel singularity with the accompanying change in the density function. It also helps provide physical interpretation of the density functions in the four different layers of potential functions introduced above. For example, the density functions for the single layer (10) of dislocations gives the gradient of dislocation and that for the double layer (9) of force dipoles gives the resultant force (per unit thickness) along the boundary. Of interest to our present application are the single layer of point forces, (8) with $k = -\kappa$ and $\Gamma(s) = t(s)/2\pi(\kappa+1)$, and the double layer of dislocation dipoles, (9) with $k = 1$ and $\gamma(s) = i\mu b(s)/\pi(\kappa+1)$, where $t(s) = t_x + it_y$ is the traction and $b(s) = b_x + ib_y$ is the Burgers vector of the dislocation.

3. Complex variable formulation of the BEM

3.1. Physical interpretation of Somigliana's identity

Consider a finite two-dimensional elastic body R whose boundary ∂R is subject to the traction $T = T_x + iT_y$ and the displacement $U = U_x + iU_y$. According to a physical interpretation [4,5] of Somigliana's identity the displacement field in this body is obtained by assuming that the region R is embedded in an infinite medium and ∂R, which is simply a line marked out in the infinite domain, is covered by a continuous distribution of point forces with density T and by a continuous distribution of dislocation dipoles with the Burgers vector U. We arrive at the physical interpretation with the help of the following imaginary series of cutting, stressing, scraping and welding operations. First, cut around the region R and remove it from the outside region R^-. Then, apply the original set of loading to the region R. This results in the traction T and the displacement U on the boundary giving rise to the final displacement field in the region. The outside region R^- is undeformed. In order to accommodate the deformed region R back in the hole, scrape away material from the surface of the hole in R^- where interpenetration is expected and fill in material where gap occurs, put the deformed region R back in the hole and rejoin the material. A pair of boundary points, one in R and another in R^-, which were coincident before the set of operations are now separated thus giving rise to a displacement discontinuity whose magnitude is equal to that for the displacement on the boundary of the region. The entire array of such discontinuities results in a layer of dislocation dipoles along the interface of the two regions. The applied traction has become built in as a layer of point forces along the interface. During the last scraping and welding operation the state of deformation in the two regions is unaltered. Thus, the displacement field in the inside region is the same as that in the finite body R and outside region R^- is undeformed. This physical interpretation of Somigliana's identity is the foundation of our direct formulation of the boundary element method in complex variables.

In our formulation the boundary integrals are evaluated analytically. We consider either a finite or infinite region R bounded by a closed contour ∂R which is subject to the traction T and the displacement U. The positive direction of the boundary ∂R is defined such that the material region is located to the left. We discretize and approximate the original boundary by a set of straight lines,

$$\partial R \approx \sum_{j=1}^{M} L_j, \tag{11}$$

where $L_j = \xi_j \xi_{j+1}$ $(j = 1, 2, \ldots, M)$ is the jth boundary element extending from nodes ξ_j to ξ_{j+1} with the slope ϕ_j as shown in Fig. 1(a).

3.2. Analytical integration for discretized layers

Consider the continuous distribution of point forces over the boundary element $L \equiv L_j$ (subscript j is omitted below) with end points ξ_1, ξ_2, and mid point ξ_3. We interpolate $\Gamma(s)$ and $\gamma(s)$ with quadratic polynomials according to

$$\Gamma(s) = \sum_{\alpha=1}^{3} \varphi_\alpha(\xi)\Gamma_\alpha, \qquad \gamma(s) = \sum_{\alpha=1}^{3} \varphi_\alpha(\xi)\gamma_\alpha, \tag{12}$$

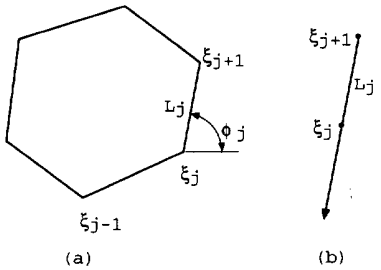

Fig. 1. (a) Approximate polygonal boundary and (b) branch cut of $\log(z - \xi)$ for element $L_j = \xi_j \xi_{j+1}$.

where $\varphi_\alpha(\xi)$ ($\alpha = 1,2,3$) are quadratic shape functions defined by Lagrange interpolation polynomials and Γ_α and γ_α are values of the density functions at collocation points ξ_α^*. Note that $\xi_3^* = \xi_3$ for the mid node, but the selection $\xi_\alpha^* \neq \xi_\alpha$ for end nodes introduces the discontinuous boundary element. The results below are valid for both continuous and discontinuous boundary elements.

The analytic integration of the single layer potential functions (8) with the interpolation (12) is given by

$$\boldsymbol{\phi}^{(s)}(z) = \sum_{\alpha=1}^{3} \mathcal{A}_\alpha^{(s)}(z)\Gamma_\alpha^*, \qquad \boldsymbol{\psi}^{(s)}(z) = \sum_{\alpha=1}^{3} \left[\mathcal{B}_\alpha^{(s)}(z)\Gamma_\alpha^* + \overline{\mathcal{C}_\alpha^{(s)}(z)\Gamma_\alpha^*}\right], \tag{13}$$

where

$$\mathcal{A}_\alpha^{(s)}(z) = -\sum_{p=1}^{3}(-1)^{p-1}\left[\varphi_\alpha^{(p-1)}(\xi)\log^{(p)}(z-\xi)\right]_{\xi_1}^{\xi_2},$$

$$\mathcal{B}_\alpha^{(s)}(z) = -\sum_{p=1}^{3}(-1)^{p-1}\left[\varphi_\alpha^{(p-1)}(\xi)\left\{\bar{\xi}\log^{(p-1)}(z-\xi) - pe^{-2i\phi}\log^{(p)}(z-\xi)\right\}\right]_{\xi_1}^{\xi_2},$$

$$\mathcal{C}_\alpha^{(s)}(z) = -\sum_{p=1}^{3}(-1)^{p-1}ke^{2pi\phi}\left[\varphi_\alpha^{(p-1)}(\xi)\overline{\log^{(p)}(z-\xi)}\right]_{\xi_1}^{\xi_2},$$

and $k = -\kappa$, $\Gamma_\alpha^* = \Gamma_\alpha e^{-i\phi}$, and $\varphi_\alpha^{(p)}(\xi)$ is the pth derivative of $\varphi_\alpha(\xi)$ with respect to ξ. The function $\log^{(p)}(z-\xi)$ is the pth integral of $\log(z-\xi)$ with respect to ξ and the branch of the complex logarithm is defined by the branch cut along the boundary element in its negative direction as shown in Fig. 1(b). The integration of the double layer potential functions (9) is given by

$$\boldsymbol{\phi}^{(d)}(z) = \sum_{\alpha=1}^{3} \mathcal{A}_\alpha^{(d)}(z)\gamma_\alpha, \qquad \boldsymbol{\psi}^{(d)}(z) = \sum_{\alpha=1}^{3} \left[\mathcal{B}_\alpha^{(d)}(z)\gamma_\alpha + \overline{\mathcal{C}_\alpha^{(d)}(z)\gamma_\alpha}\right], \tag{14}$$

where

$$\mathcal{A}_\alpha^{(d)}(z) = -\sum_{p=0}^{2}(-1)^{p}\left[\varphi_\alpha^{(p)}(\xi)\log^{(p)}(z-\xi)\right]_{\xi_1}^{\xi_2},$$

$$\mathcal{B}_\alpha^{(d)}(z) = -\sum_{p=0}^{2}(-1)^{p}\left[\varphi_\alpha^{(p)}(\xi)\left\{\bar{\xi}\log^{(p-1)}(z-\xi) - p\,e^{-2i\phi}\log^{(p)}(z-\xi)\right\}\right]_{\xi_1}^{\xi_2},$$

$$\mathcal{C}_\alpha^{(d)}(z) = -\sum_{p=0}^{2}(-1)^{p}k\,e^{2pi\phi}\left[\varphi_\alpha^{(p)}(\xi)\overline{\log^{(p)}(z-\xi)}\right]_{\xi_1}^{\xi_2},$$

and $k = 1$.

Substitution of (13) and (14) into (1) and (3) will give the displacement contribution in the form

$$2u^{(s)}(z) = \sum_{\alpha=1}^{3}\left[M_\alpha(z)\frac{T_\alpha}{\mu} + \overline{N_\alpha(z)\frac{T_\alpha}{\mu}}\right], \qquad 2u^{(d)}(z) = \sum_{\alpha=1}^{3}\left[K_\alpha(z)U_\alpha + \overline{L_\alpha(z)U_\alpha}\right], \tag{15}$$

and the traction contribution in the form

$$t^{(s)}(z) = \sum_{\alpha=1}^{3}\left[M_\alpha^*(z)T_\alpha + \overline{N_\alpha^*(z)T_\alpha}\right], \qquad t^{(d)}(z) = \mu\sum_{\alpha=1}^{3}\left[K_\alpha^*(z)U_\alpha + \overline{L_\alpha^*(z)U_\alpha}\right], \tag{16}$$

for the single and double layers, respectively [34]. Following the physical interpretation of Somigliana's identity, the actual displacement and the traction are given by the sums

$$2u(z) = 2u^{(s)}(z) + 2u^{(d)}(z), \qquad t(z) = t^{(s)}(z) + t^{(d)}(z).$$

Before formulating the boundary equations it is necessary to extract the real and the imaginary parts of the displacement and traction and then follow the standard procedure of the BEM to obtain either the system of displacement or the traction boundary equations [34].

4. Crack source method for center cracks

4.1. Single center crack in the infinite body

Consider the Chebyshev polynomials, $T_m(x)$ and $U_{m-1}(x)$, of the first and second kind and define, as in [35], two Cauchy-type integrals

$$T^{(m)}(z) = -\frac{1}{\pi}\int_{-1}^{1} \frac{\sqrt{1-x^2}U_{m-1}(x)\,dx}{x-z} \quad (m \geqslant 0),$$
$$U^{(m-1)}(z) = \frac{1}{\pi}\int_{-1}^{1} \frac{T_m(x)\,dx}{\sqrt{1-x^2}(x-z)} \quad (m \geqslant 0), \tag{17}$$

where $z = x + iy$ is a complex variable. These integrals are evaluated analytically, using the Cauchy integral formula, with the result

$$T^{(m)}(z) = \left(z - \sqrt{z^2-1}\right)^m \quad (m \geqslant 0),$$
$$U^{(m-1)}(z) = -\frac{\left(z - \sqrt{z^2-1}\right)^m}{\sqrt{z^2-1}} \quad (m \geqslant 0). \tag{18}$$

Note that $T^{(0)}(z) = 1$ and $U^{(-1)}(z) = -1/\sqrt{z^2-1}$.

A dislocation dipole with the Burgers vector b defined over an infinitesimal segment $d\xi$ is the source of displacement discontinuity over $d\xi$. When the displacement discontinuity is identified as the crack opening displacement we call the dipole as the crack source. The continuous distribution of the crack sources over an arc C is called the crack element. We consider a straight center crack C and introduce a local coordinate system O-xy by placing the coordinate origin O at the crack center and the x-axis along the crack so that the crack lies in the interval $(-a, a)$ as shown in Fig. 2(a). The complex variable in this coordinate system is denoted by $z = x + iy$ and the crack opening displacement by $\delta = \delta_x + i\delta_y$. In order to obtain the normalized crack interval $(-1, +1)$ let $Z = z/a$ (i.e. $X = x/a$ and $Y = y/a$), then the complex potential functions of the crack element C are given, from (9) with $k = 1$, by

$$\phi^{(d)}(Z) = \int_{-1}^{+1} \tilde{\gamma}(X)\frac{dX}{Z-X},$$
$$\psi^{(d)}(Z) = \int_{-1}^{+1} \left\{\tilde{\gamma}(X) + \overline{\tilde{\gamma}(X)}\right\}\frac{dX}{Z-X} - \frac{\partial}{\partial Z}\left\{\int_{-1}^{+1} \tilde{\gamma}(X)\frac{X\,dX}{Z-X}\right\}, \tag{19}$$

where

$$\tilde{\gamma}(X) = \gamma(x) = i\mu\delta/\pi(\kappa+1).$$

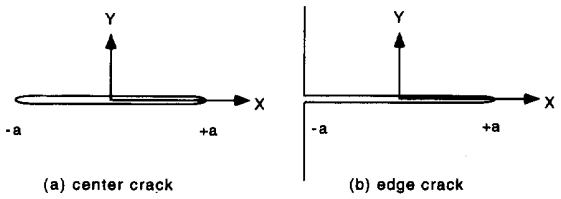

Fig. 2. (a) Local coordinate system for a center crack and (b) for an edge crack.

In order to embed the known crack tip opening displacement behavior into the problem we interpolate the density function $\tilde{\gamma}(X)$ by

$$\tilde{\gamma}(X) = \frac{i\mu}{\pi(\kappa+1)}\sqrt{1-X^2}\sum_{m=1}^{p}\delta^{(m)}U_{m-1}(X). \tag{20}$$

If we use (19), the integrals in (19) with (20) can be evaluated analytically with the result

$$\begin{aligned}\phi^{(d)}(Z) &= \frac{i\mu}{(\kappa+1)}\sum_{m=1}^{p}\delta^{(m)}T^{(m)}(Z),\\ \psi^{(d)}(Z) &= -\frac{i\mu}{(\kappa+1)}\sum_{m=1}^{p}\left\{\overline{\delta^{(m)}}T^{(m)}(Z)+m\delta^{(m)}ZU^{(m-1)}(Z)\right\}.\end{aligned} \tag{21}$$

The displacement contribution is given, from (21) and (1), by

$$2(u_x+iu_y) = \sum_{m=1}^{p}\left(K^{(m)}(Z)\delta^{(m)}+\overline{L^{(m)}(Z)\delta^{(m)}}\right), \tag{22}$$

where

$$\begin{aligned}K^{(m)}(Z) &= \frac{i}{\kappa+1}\left\{\kappa T^{(m)}(Z)-\overline{T^{(m)}(Z)}\right\},\\ L^{(m)}(Z) &= \frac{i}{\kappa+1}(Z-\overline{Z})mU^{(m-1)}(Z),\end{aligned} \tag{23}$$

and the stress contribution, from (21) and (2), by

$$\frac{\sigma_{xx}+\sigma_{yy}}{2} = \frac{2\mu}{a(\kappa+1)}\operatorname{Re}\left\{i\sum_{m=1}^{p}m\delta^{(m)}U^{(m-1)}(Z)\right\}, \tag{24}$$

$$\begin{aligned}\frac{\sigma_{yy}-\sigma_{xx}}{2}+i\sigma_{jxy} = -\frac{i\mu}{a(\kappa+1)}\sum_{m=1}^{p}\Bigg[&+m(\delta^{(m)}+\overline{\delta^{(m)}})U^{(m-1)}(Z)\\ &+m\delta^{(m)}\frac{Z-\overline{Z}}{Z^2-1}\left\{(m+1)T^{(m)}(Z)-U^{(m)}(Z)\right\}\Bigg].\end{aligned}$$

The traction on the line segment with the slope θ is given, from (21) and (3), by

$$t_x+it_y = \mu\sum_{m=1}^{p}\left\{K^{*(m)}(Z,\theta)\delta^{(m)}+\overline{L^{*(m)}(Z,\theta)\delta^{(m)}}\right\}, \tag{25}$$

where

$$\begin{aligned}K^{*(m)}(Z,\theta) &= \frac{m}{a(\kappa+1)}\left\{e^{i\theta}U^{(m-1)}(Z)+e^{-i\theta}\overline{U^{(m-1)}(Z)}\right\},\\ L^{*(m)}(Z,\theta) &= \frac{m}{a(\kappa+1)}\left\{\left(e^{i\theta}-e^{-i\theta}\right)U^{(m-1)}(Z)+e^{i\theta}\frac{Z-\overline{Z}}{Z^2-1}\left[(m+1)T^{(m)}(Z)-U^{(m)}(Z)\right]\right\}.\end{aligned} \tag{26}$$

Of interest is the traction along the crack line, which is given by

$$(t_x+it_y)^{+} = \frac{2\mu}{a(\kappa+1)}\sum_{m=1}^{p}m\delta^{(m)}U_{m-1}(X)\quad(|X|\leqslant 1), \tag{27}$$

on the upper crack surface and the stress on the X-axis outside the crack

$$\sigma_{yy}+i\sigma_{xy} = \pm\frac{2\mu i}{a(\kappa+1)}\sum_{m=1}^{p}m\overline{\delta^{(m)}}\frac{\left(X\mp\sqrt{X^2-1}\right)^m}{\sqrt{X^2-1}}, \tag{28}$$

where the upper and lower signs correspond to $X > 1$ and $X < -1$, respectively. The stress intensity factor is extracted, from (28), as

$$K(\pm 1) = K_{\mathrm{I}}(\pm 1) + iK_{\mathrm{II}}(\pm 1) = \frac{2\mu i}{\kappa + 1}\sqrt{\frac{\pi}{a}}\sum_{m=1}^{p}(\pm 1)^{m+1} m\overline{\delta^{(m)}}, \tag{29}$$

where K_{I} and K_{II} are the Mode I and II stress intensity factors in the local O-xy coordinate system.

The solution when the traction is specified on the crack surface, is obtained from (27), by the traction collocation on the crack surface. Consider, as a special case, the traction free crack in the infinite body subject to the remote loading specified by the complex potential functions $\phi_\infty(z)$ and $\psi_\infty(z)$. We seek the solution in the form

$$\phi(z) = \phi_\infty(z) + \phi_o(z), \qquad \psi(z) = \psi_\infty(z) + \psi_o(z). \tag{30}$$

The additional complex potential functions $\phi_0(z)$ and $\psi_0(z)$ are required to satisfy the traction free boundary condition

$$t = t_\infty + t_0 = 0,$$

on the crack surface, where t_∞ and t_0 are the remote and the additional traction contributions, respectively. This homogeneous traction boundary condition can be rewritten as a non-homogeneous one

$$t_0 = -t_\infty, \tag{31}$$

which is used in the solution of $\phi_0(z)$ and $\psi_0(z)$. The argument presented above is the basis of the method of superposition for the crack and hole problems in the infinite body which will be used below for multiple crack problems.

Unlike the quadrature formula for the singular integrals, where the selection of quadrature and collocation points must strictly obey a certain rule [27,28], our selection of the collocation point on the crack surface is arbitrary. The best result is obtained by including the crack tips among the collocation points; as seen from (27), the traction on the crack surface is bounded at the crack tip allowing its evaluation. Contrast this with the numerical quadrature that must avoid the crack tip as a collocation point. The advantage of the current method is that the stress intensity factors are calculated directly by the formula (29) without the need for indirect means to calculate them.

4.2. Multiple center cracks

All the necessary ingredients for the solution of multiple center cracks are already present in the solution of the single crack. Additional step needed to accommodate multiple cracks is the introduction of multiple coordinate systems. Fig. 3 shows the coordinate systems used in the formulation. Each crack has its own local coordinate system O_j-x_jy_j ($j = 1, \ldots, N$) in which the x_j-axis is aligned with the crack. In addition, the global coordinate system O-xy is used to specify the crack geometry by its center, inclination, and length.

For each crack we convert the global crack geometry into local geometry associated with the local coordinate system, where the crack is placed on the local x_j-axis. The traction contribution from each

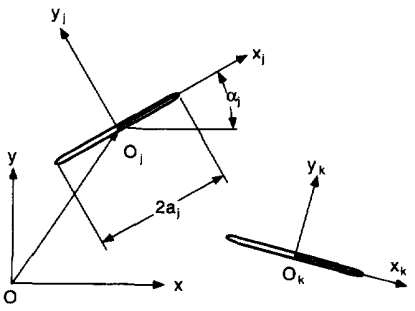

Fig. 3. Coordinate systems used in the formulation of multiple cracks.

crack is calculated by (27) and (25) depending on whether the observation point Z is located on the crack surface itself or not; the latter is used to calculate the traction contribution at other crack sites. Finally, the actual traction on each crack surface is obtained by adding contributions from all existing cracks including itself; the addition must be performed for the traction component defined in the global coordinate system. Let t_{local} be the traction contribution from one of the cracks given in the local coordinate system and let the slope of the local x_j-axis be α, then the same traction in the global coordinate system is given by

$$t_{\text{global}} = \mathrm{e}^{\mathrm{i}\alpha} t_{\text{local}}.$$

The unknown crack opening coefficients $\delta^{(m)}$ in (20) are determined by the traction collocation on each crack surface.

By combining the BEM and the crack source method modules presented earlier we can now handle multiple center cracks in arbitrarily shaped finite bodies. These two modules must be coupled so that the effects of the cracks are considered on the non-crack boundary and the vice versa. We calculate the displacement on the non-crack boundary and traction on the crack surfaces. Since the non-crack boundary does not intersect with any of the cracks we can use the continuous boundary elements.

5. Crack source method for edge cracks

Consider an edge crack and introduce the local coordinate system along the crack as shown in Fig. 2(b). Without a loss of generality we assume the crack tip at $x = a$ and the crack mouth at $x = -a$; the opposite case can easily be handled. We propose to interpolate the density function $\tilde{\gamma}(X)$ for an edge crack in two parts. The singular part

$$\tilde{\gamma}_s(X) = \frac{\mathrm{i}\mu}{\pi(\kappa+1)} (1-X)^{\alpha}(1+X)^{\beta} \sum_{m=1}^{p} \delta^{(m)} P_{m-1}^{(\alpha,\beta)}(X), \tag{32}$$

where $P_m^{(\alpha,\beta)}(X)$ is the Jacobi polynomial, captures the exact crack tip opening displacement behavior with the choice of $\alpha = 1/2$. The value of β is selected such that no stress singularity arises at the crack mouth; the convenient but arbitrary choice is $\beta = 3/2$ which satisfies an additional condition described below. This selection of β constrains the slope contribution at the crack mouth to zero; although this is not physically quite correct a study in [36] has shown its negligible effect on the stress intensity factor. In addition, the slope there is modified by the regular part considered below anyway. The regular part

$$\tilde{\gamma}_r(X) = \frac{\mathrm{i}\mu}{\pi(\kappa+1)} \sum_{n=1}^{q} \Delta^{(n)} (1-X)^n, \tag{33}$$

provides the non-zero crack mouth opening displacement. Analytic evaluation of the potential functions (19) with the singular part (32) depends on the evaluation of the integrals:

$$R^{(m)}(z) = -\frac{1}{\pi} \int_{-1}^{+1} \frac{(1-x)^{\alpha}(1+x)^{\beta} P_{m-1}^{(\alpha,\beta)}(x)\,\mathrm{d}x}{x-z},$$

$$G^{(m-1)}(z) = \frac{1}{\pi} \int_{-1}^{+1} \frac{(1-x)^{\alpha-1}(1+x)^{\beta-1} P_m^{(\alpha-1,\beta-1)}(x)\,\mathrm{d}x}{x-z},$$

which, with the help of the Cauchy integral formula, is possible with the result

$$R^{(m)}(z) = -\frac{1}{\sin \pi\alpha} \left\{ P_{m-1}^{(\alpha,\beta)}(z)(z-1)^{\alpha}(z+1)^{\beta} - 2^{\alpha+\beta} P_{m-1+\alpha+\beta}^{(-\alpha,-\beta)}(z) \right\},$$

$$G^{(m-1)}(z) = -\frac{1}{\sin \pi\alpha} \left\{ P_m^{(\alpha-1,\beta-1)}(z)(z-1)^{\alpha-1}(z+1)^{\beta-1} - 2^{\alpha+\beta-2} P_{m-2+\alpha+\beta}^{(1-\alpha,1-\beta)}(z) \right\}, \tag{34}$$

where $\alpha + \beta$ must be an integer but otherwise arbitrary, $m \geqslant 1$, and z is a complex variable.

Analytical integration of the complex potential functions (19) with the singular part (32) is given, using (34), by

$$\phi^{(d)}(Z) = \frac{i\mu}{(\kappa+1)} \sum_{m=1}^{p} \delta^{(m)} R^{(m)}(Z),$$

$$\psi^{(d)}(Z) = -\frac{i\mu}{(\kappa+1)} \sum_{m=1}^{p} \left\{ \overline{\delta^{(m)}} R^{(m)}(Z) + 2m\delta^{(m)} Z G^{(m-1)}(Z) \right\}. \tag{35}$$

The displacement, stress, and traction contributions can readily be calculated by these potential functions by substituting (35) into (1), (2) and (3). The explicit formula for the stress intensity factor contribution comes from the singular part (32) as given by

$$K_I + iK_{II} = \frac{2\mu i}{\kappa+1} 2^{\beta+\alpha} \sqrt{\frac{\pi}{a}} \sum_{m=1}^{p} m P_m^{(\alpha-1,\beta-1)}(1) \overline{\delta^{(m)}}, \tag{36}$$

where K_I and K_{II} are Mode I and II stress intensity factors, $\alpha = 1/2$, and $\beta = 3/2$. There is no need to obtain the stress intensity factor by extrapolation method or other indirect methods such as the J integral. The treatment of the regular part (33) essentially follows that for the ordinary polynomial interpolation for the BEM and will not be discussed further. The process involved in extending the single edge crack results to multiple edge cracks problems parallels that for the center cracks.

Unlike many center crack problems the presence of non-crack boundary, thus the coupling with the BEM is the integral part of the edge crack problems. Especially important is the requirement of displacement compatibility: the displacement jump experienced by the boundary element nodes across the crack mouth must be equal to the crack opening displacement there. For the boundary elements that intersect a crack, discontinuous elements may be used to relax the requirement of displacement compatibility at the crack mouth; in reality the solution by the discontinuous elements at the crack mouth satisfies the compatibility condition extremely well. For edge cracks the collocation points can still be selected arbitrarily excluding the crack tip and crack mouth, where the traction contribution from the regular part (33) becomes unbounded.

6. Numerical results

We have analyzed fifteen problems in this paper. Each problem has zero traction on the crack surface. For all the center crack problems 7 Chebyshev polynomials have been used and for all the edge crack problems 3 singular and 8 regular terms ($p = 3$ and $q = 8$) have been used. The collocation points on the crack surface have been placed uniformly.

Figs. 4–6 show two collinear cracks, two parallel cracks, and three parallel cracks, respectively, in the infinite body under uniaxial tension. The solution is obtained by the method of superposition using the remote potential functions. Comparison of our numerical results and the results from the stress intensity Handbook [37] are listed in Tables 1–3, respectively. Figs. 7 and 8 show two parallel cracks with an offset and two inclined cracks, respectively, in the infinite body in uniaxial tension. Our numerical results listed in Tables 4 and 5 are in good agreement with the Handbook [37] results, which provides only the stress intensity factor curves for the two problems.

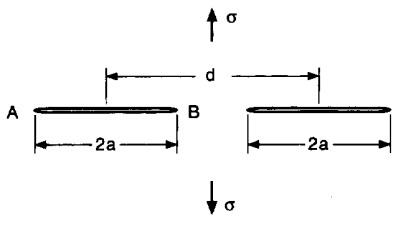

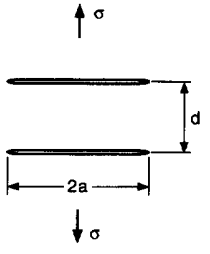

Fig. 4. Two collinear cracks in the infinite body under uniaxial tension.
Fig. 5. Two parallel cracks in the infinite body under uniaxial tension.

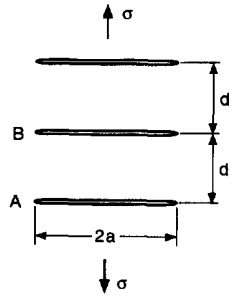

Fig. 6. Three parallel cracks in the infinite body under uniaxial tension.

Table 1
Stress intensity factors for two collinear cracks in the infinite body

$2a/d$	$K_{IA}/\sigma\sqrt{\pi a}$		$K_{IB}/\sigma\sqrt{\pi a}$	
	Ref. [37]	Present	Ref. [37]	Present
0.05	1.00031	1.0018	1.00032	1.0018
0.1	1.0012	1.0027	1.0013	1.0028
0.2	1.0046	1.0061	1.0057	1.0071
0.3	1.0102	1.0117	1.0138	1.0153
0.4	1.0179	1.0194	1.0272	1.0287
0.5	1.0280	1.0295	1.0480	1.0495
0.6	1.0410	1.0426	1.0804	1.0821
0.7	1.0579	1.0596	1.1333	1.1351
0.8	1.0811	1.0827	1.2289	1.2314
0.9	1.1174	1.1187	1.4539	1.4639

Table 2
Stress intensity factors for two parallel cracks in the infinite body

$2a/d$	$K_I/\sigma\sqrt{\pi a}$	
	Ref. [37]	Present
0.0	1.0000	1.0011
0.2	0.9855	0.9870
0.4	0.9508	0.9517
0.8	0.8727	0.8732
1.0	0.8319	0.8440
2.0	0.7569	0.7746
5.0	0.6962	0.7129

Table 3
Stress intensity factors for three parallel cracks in the infinite body

$2a/d$	$K_{IA}/\sigma\sqrt{\pi a}$		$K_{IB}/\sigma\sqrt{\pi a}$
	Ref. [37]	Present	Present
0.1	0.99500	0.99687	0.99410
0.2	0.98198	0.98379	0.97306
0.3	0.96299	0.96430	0.94156
0.4	0.94010	0.94100	0.90361
0.5	0.91535	0.91650	0.86789
0.6	0.89080	0.89254	0.82333
0.7	0.86851	0.87041	0.78603
0.8	0.85052	0.85062	0.75234

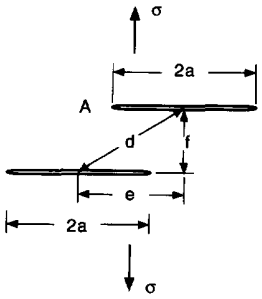

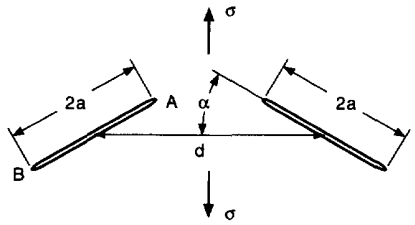

Fig. 7. Two parallel cracks in the infinite body with an offset under uniaxial tension.

Fig. 8. Two inclined cracks in the infinite body under uniaxial tension.

Table 4
Stress intensity factors for two parallel cracks with an offset in the infinite body

$2a/d$	$K_{IA}/\sigma\sqrt{\pi a}$ (Present)			
	e/f=1	e/f=2	e/f=3	e/f=10
0.1	1.00269	1.00345	1.00326	1.00287
0.2	1.00581	1.00982	1.00911	1.00743
0.3	1.00959	1.02154	1.02029	1.01604
0.4	1.01182	1.03960	1.03875	1.03025
0.5	1.00928	1.06455	1.06742	1.05271
0.6	0.99831	1.09482	1.10971	1.08861
0.7	0.97610	1.12381	1.16940	1.14941
0.8	0.94208	1.13712	1.23706	1.26639
0.9	0.89841	1.11657	1.27650	1.53904

Table 5
Stress intensity factors for two inclined cracks in the infinite body, where $F_{IA} = K_{IA}/\sigma\sqrt{\pi a}$ and $F_{IB} = K_{IB}/\sigma\sqrt{\pi a}$ are defined locally along the crack line

$2a/d$	Present					
	20°		30°		60°	
	F_{IA}	F_{IB}	F_{IA}	F_{IB}	F_{IA}	F_{IB}
0.1	0.8847	0.8847	0.7503	0.7503	0.2469	0.2469
0.2	0.8877	0.8866	0.7522	0.7516	0.2470	0.2460
0.3	0.8934	0.8900	0.7559	0.7534	0.2474	0.2447
0.4	0.9027	0.8956	0.7620	0.7560	0.2490	0.2427
0.5	0.9175	0.9023	0.7718	0.7595	0.2518	0.2402
0.6	0.9404	0.9108	0.7871	0.7640	0.2562	0.2375
0.7	0.9767	0.9218	0.8110	0.7698	0.2623	0.2346
0.8	1.0382	0.9363	0.8490	0.7775	0.2702	0.2321
0.9	1.1600	0.9570	0.9140	0.7881	0.2799	0.2298

Fig. 9(a) shows an inclined center crack in an infinite strip under uniaxial tension. Unlike the previous problems the effects of the finitely located boundary come into play. A long strip with the length twenty times the width has been selected to simulate the infinite strip. The mesh with 28 boundary elements is shown in Fig. 9(b). The stress intensity factor results are shown in Figs. 9(c) and 9(d) in comparison with those in the Handbook [37]. Fig. 10(a) shows a slant crack in a rectangular plate subject to parabolic tensile loading. We have discretized each side of the plate with 10 uniform boundary elements. The stress intensity factors obtained are plotted in Fig. 10(b) and compared with the curves from the Handbook [37].

In order to examine the effects of discontinuous elements at the crack mouth for edge cracks, we have selected a test problem of a double edge cracked finite plate in uniaxial tension. Figs. 11(a) and 11(b)

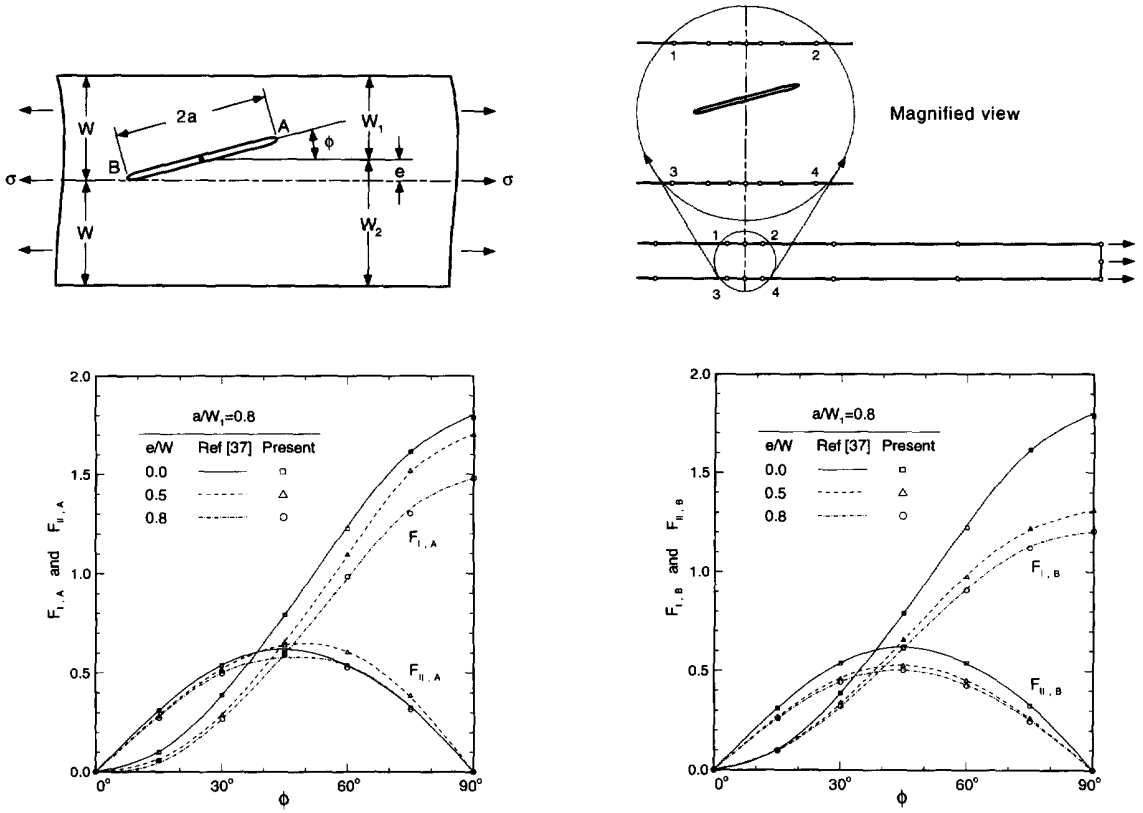

Figure 9 . (a) An inclined crack in an infinite strip under tension; (b) mesh used for an inclined crack in an infinite strip under tension; (c) stress intensity factors for an inclined crack in an infinite plate under tension: for crack tip A with $F_{I,A} = K_{I,A}/\sigma\sqrt{\pi a}$ and $F_{II,A} = K_{II,A}/\sigma\sqrt{\pi a}$; (d) stress intensity factors for an inclined crack in an infinite plate under tension: for crack tip B with $F_{I,B} = K_{I,B}/\sigma\sqrt{\pi a}$ and $F_{II,B} = K_{II,B}/\sigma\sqrt{\pi a}$.

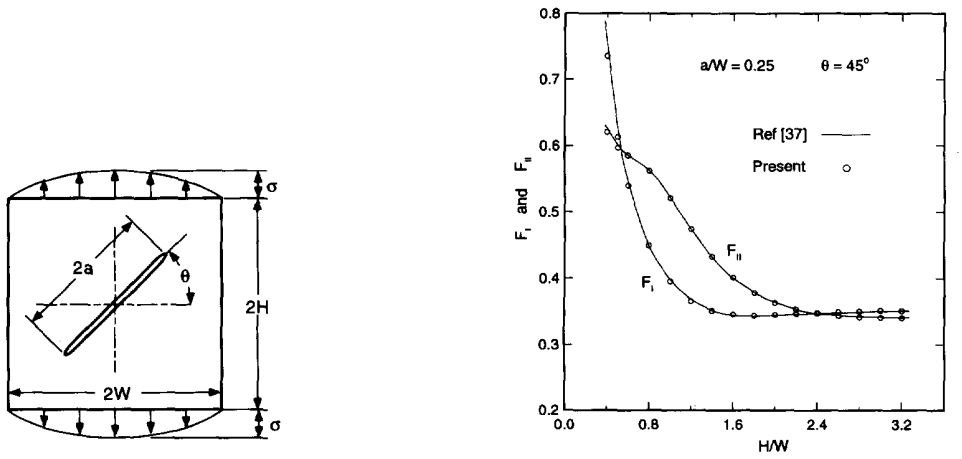

Figure 10 . (a) Center slant cracked rectangular plate under parabolic tension; (b) stress intensity factors for a center slant cracked rectangular plate under parabolic tension with $F_I = K_I/\sigma\sqrt{\pi a}$ and $F_{II} = K_{II}/\sigma\sqrt{\pi a}$.

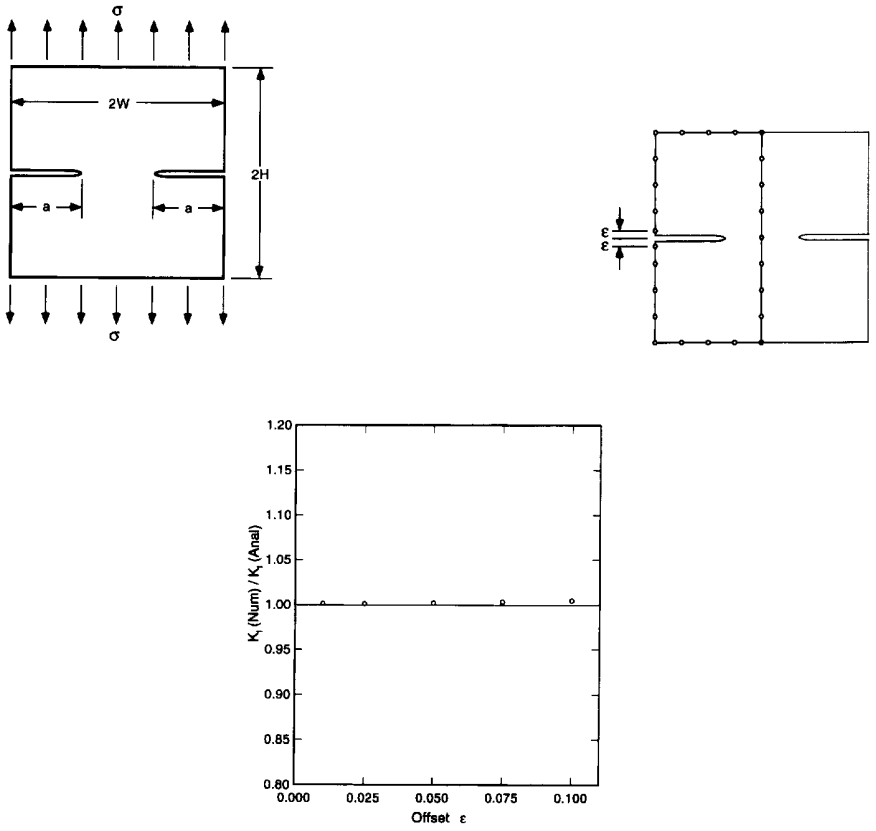

Figure 11 . (a) Double edge crack in a rectangular plate in uniaxial tension; (b) mesh for the double edge crack (24 elements are shown) with the offset ϵ for discontinuous elements; (c) effects of the offset ϵ on the stress intensity factor.

show the specimen geometry and boundary element mesh, respectively. Exploiting the symmetry only one half of the plate is analyzed using 24 uniform elements. The offset ϵ in the discontinuous boundary element from the crack surface, as shown in Fig. 11(b), has been varied from $\epsilon = 0.01$ to 0.1 in the local element coordinate system ranging from -1 to $+1$. Fig. 11(c) shows the stress intensity factor results against ϵ, which remain practically constant.

The numerical results for a slanted edge crack in a finite rectangular plate shown in Fig. 12(a) are listed in Figs. 12(b) and 12(c) along with the curves obtained from the Handbook [37]. The number of boundary elements used is 48. Fig. 13(a–d) show cracks emanating from a triangular or a square hole in the infinite body subject to uniaxial tension. The stress intensity factor results have been obtained by the method of superposition involving the potential functions for the remote loading. On each hole 16 boundary elements were used. Comparison of our numerical results and the Handbook values are given in Tables 6(a–d). Note that our numerical results stay within 1 per cent of the Handbook values and that the Handbook lists the accuracy of the results, for these four problems, to be 1%.

We have analyzed two half-plane edge crack problems whose accuracy is known to be within 0.1%, according to the Handbook [37]. Fig. 14(a) shows two edge cracks and Fig. 15 an edge crack at a corner of a rectangular notch in the half-plane subject to tension. We have used 26 meshes for the former and 34 for the latter. Fig. 14(b) shows the mesh for the two edge cracks problem that progressively become coarser as we move away from the cracked region. Similar non uniform mesh has been used for the second problem. The stress intensity factor results are listed in Tables 7(a), 7(b), and 8. The majority of the values stay within 0.1% of the Handbook values whose accuracy is reported to be 0.1%.

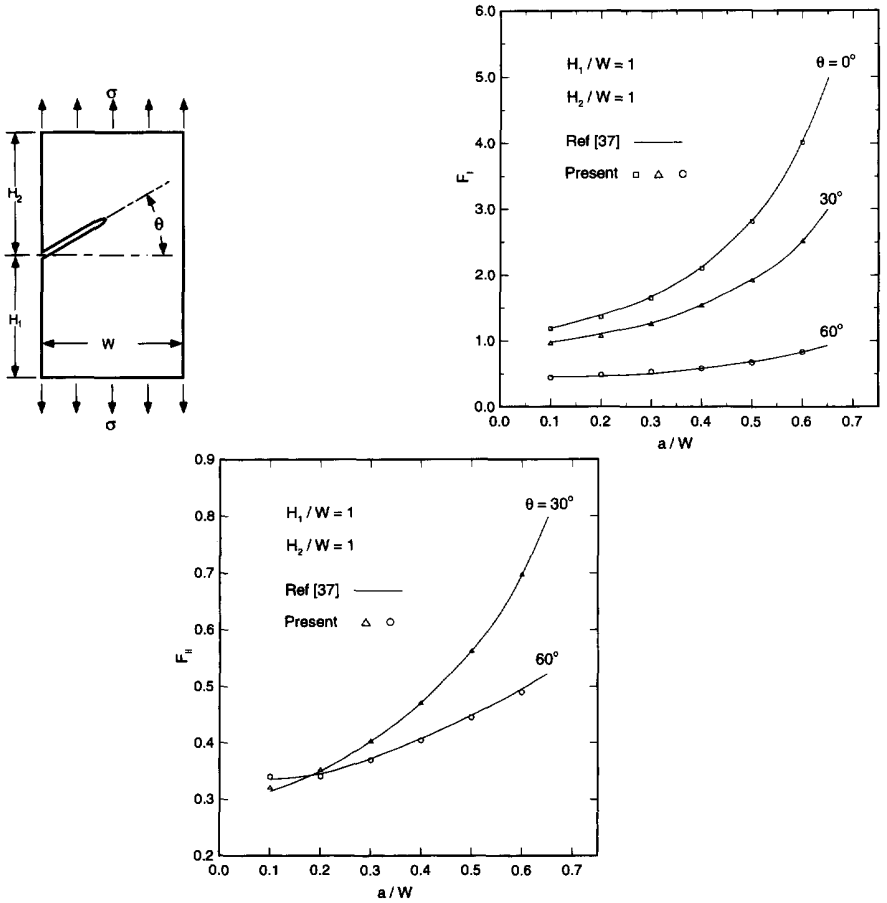

Figure 12 . (a) Edge slant crack in a rectangular plate in a rectangular plate in uniaxial tension; (b) mode I stress intensity factors for edge slant crack in a rectangular plate in uniaxial tension with $F_{\mathrm{I}} = K_{\mathrm{I}}/\sigma\sqrt{\pi a}$; (c) mode II stress intensity factors for edge slant crack in a rectangular plate in uniaxial tension with $F_{\mathrm{II}} = K_{\mathrm{II}}/\sigma\sqrt{\pi a}$.

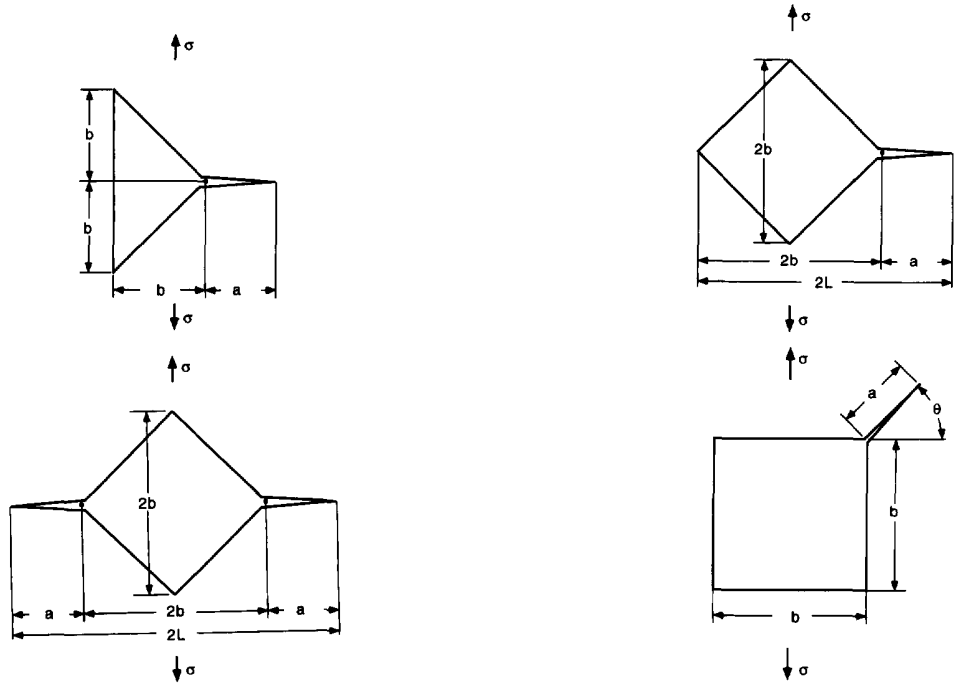

Figure 13 . (a) An edge crack emanating from a triangular hole in the infinite body under uniaxial tension; (b) an edge crack emanating from a square hole in the infinite body under uniaxial tension; (c) two edge cracks emanating from a square hole in the infinite body under uniaxial tension; (d) an edge crack at a corner of a square hole in the infinite body under uniaxial tension.

Table 6

(a) Stress intensity factors for an edge crack emanating from a triangular hole in the infinite body under uniaxial tension

a/b	$K_I/\sigma\sqrt{\pi a}$	
	Ref. [37]	Present
0.1	2.76	2.822
0.2	2.064	2.052
0.4	1.525	1.516
0.6	1.297	1.290
0.8	1.168	1.162
1.0	1.085	1.081

(b) Stress intensity factors for an edge crack emanating from a square hole in the infinite body under uniaxial tension

0.1	3.38	3.444
0.2	2.516	2.496
0.4	1.836	1.823
0.6	1.540	1.530
0.8	1.370	1.361
1.0	1.258	1.251

(c) Stress intensity factors for two edge cracks emanating from a square hole in the infinite body under uniaxial tension

0.1	1.07	1.062
0.2	1.069	1.062
0.4	1.058	1.052
0.6	1.046	1.041
0.8	1.037	1.031
1.0	1.030	1.026

(d) Stress intensity factors for an edge crack at a corner of a square hole in the infinite body under uniaxial tension

a/b	θ	$K_I/\sigma\sqrt{\pi a}$		$K_{II}/\sigma\sqrt{\pi a}$	
		Ref. [37]	Present	Ref. [37]	Present
0.2	30°	1.28	1.268	0.626	0.625
	45°	0.928	0.924	0.788	0.795
	60°	0.543	0.540	0.833	0.842

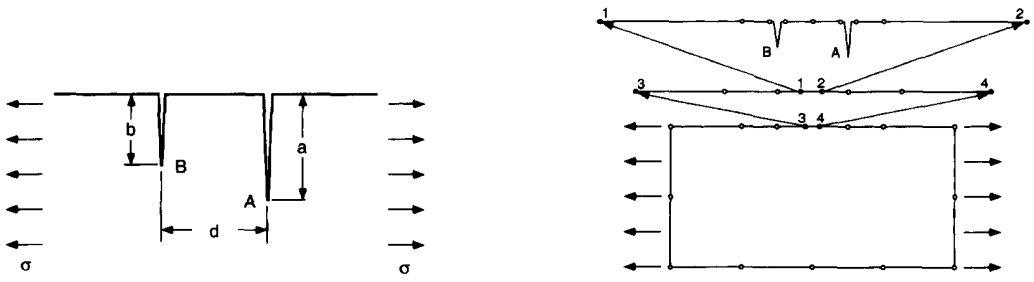

Figure 14 . (a) Two edge cracks in the semi-infinite plate under tension; (b) the mesh for two edge cracks in the semi-infinite plate under tension.

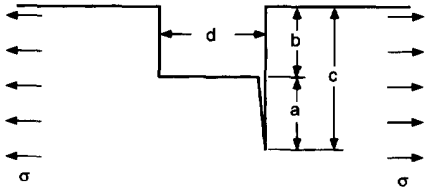

Figure 15 . Edge crack at a corner of a rectangular notch in the semi-infinite body under tension.

Table 7
(a) Stress intensity factors for two edge cracks in the semi-infinite plate under tension: Mode I with $F_{IA} = K_{IA}/\sigma\sqrt{\pi a}$, $F_{IB} = K_{IB}/\sigma\sqrt{\pi b}$

Present (Ref. [37] in parentheses)						
d/a	0.5		1.0		2.0	
b/a	F_{IA}	F_{IB}	F_{IA}	F_{IB}	F_{IA}	F_{IB}
1.0	0.825	0.825	0.854	0.854	0.909	0.909
	(0.817)	(0.817)	(0.854)	(0.854)	(0.911)	(0.911)
0.9	0.951	0.659	0.929	0.775	0.950	0.876
	(0.951)	(0.655)	(0.929)	(0.776)	(0.952)	(0.879)
0.75	1.054	0.405	1.015	0.642	1.0025	0.823
	(1.066)	(0.407)	(1.015)	(0.644)	(1.005)	(0.827)
0.5	1.119	0.114	1.093	0.414	1.067	0.737
	(1.118)	(0.118)	(1.094)	(0.418)	(1.071)	(0.738)
0.25	1.122	-0.042	1.117	0.212	1.104	0.644
	(1.122)	(-0.042)	(1.118)	(0.214)	(1.109)	(0.659)

(b) Stress intensity factors for two edge cracks in the semi-infinite plate under tension: Mode II with $F_{IIA} = K_{IIA}/\sigma\sqrt{\pi a}$, $F_{IIB} = K_{IIB}/\sigma\sqrt{\pi b}$

Present						
d/a	0.5		1.0		2.0	
b/a	F_{IIA}	F_{IIB}	F_{IIA}	F_{IIB}	F_{IIA}	F_{IIB}
1.0	-0.155	0.155	-0.132	0.132	-0.092	0.092
0.9	-0.102	0.183	-0.108	0.147	-0.079	0.095
0.75	-0.052	0.177	-0.072	0.159	-0.059	0.095
0.5	0.003	0.096	-0.024	0.145	-0.029	0.080
0.25	0.004	0.024	-0.003	0.092	-0.008	0.050

Table 8
Stress intensity factors for an edge crack at a corner of a rectangular notch in the semi-infinite body under tension

a/b	$K_I/\sigma\sqrt{\pi c}$		$K_{II}/\sigma\sqrt{\pi c}$	
	Ref. [37]	Present	Ref. [37]	Present
0.1	0.84	0.8353	-0.12	-0.1207
0.2	0.937	0.9390	-0.089	-0.0938
0.5	1.071	1.0684	-0.036	-0.0354
1.0	1.117	1.1134	-0.002	-0.0014
2.0	1.1215	1.1185	0.000	0.0031

7. Conclusion

The numerical method for multiple crack problems has been proven to be extremely accurate for fifteen problems studied in the paper. It should produce stress intensity factor results accurate enough to substitute those from stress intensity factor handbooks as long as the two-dimensional cracks in the homogeneous domain are concerned. The method can also be applied effectively for more complex real life problems than those considered in the paper. The analytical integration of the layers of potential functions defined over the cracks and non-crack boundary increases the accuracy while decreasing the computer time significantly. The implementation of the method is straightforward due to the simplicity of the resulting analytical formulas.

Acknowledgment

This work was supported by the Center for Computational Modeling of Aircraft Structures at Rutgers University.

References

[1] N.I. Muskhelishvili, Some Basic Problems of the Mathematical Theory of Elasticity (Noordhoff, Groningen, 1958).
[2] P.K. Banerjee and R. Butterfield, Boundary Element Methods in Engineering Science (McGraw-Hill, London, 1981).
[3] C.A. Brebbia and J. Dominquez, Boundary Elements: An Introductory Course (Computational Mechanics Publications, Southampton, 1989).
[4] N.J. Altiero and S.D. Gavazza, On a unified boundary-integral equation method, J. Elasticity 10(1) (1980) 1–9.
[5] M. Denda, A complex variable approach to inelastic boundary value problems, in: H. Chung et al., ed., Advances in Design and Analysis in Pressure Vessel Technology (ASME PVP—Vol. 130, NE—Vol. 2 23–32, New York, 1987).
[6] T.V. Hromadka II and C. Lai, The Complex Variable Boundary Element Method in Engineering Analysis (Springer-Verlag, New York, 1986).
[7] K.J. Lee, A boundary element method for plane isotropic elastic media using complex variable technique, Comput. Mech. 11 (1993) 83–91.
[8] I.N. Vekua, New Methods for Solving Elliptic Equations (North-Holland, Amsterdam, 1967).
[9] A.I. Kalandiya, Mathematical Methods of Two-dimensional Elasticity (Mir Publishers, Moscow, 1975).
[10] M.P. Savruk, Plane problems of the theory of elasticity for a multiply connected area with holes and cracks (in Russian). Fiz.-Khim. Mekh. Mat. 16(5) (1980) 51–56.
[11] G.E. Blandford, A.R. Ingraffea and J.A. Liggett, Two-dimensional stress intensity factor computations using the boundary element method, Int. J. Numer. Methods Engrg. 17 (1981) 387–404.
[12] G. Kuhn, Numerische behandlung von mehrfachrissen in ebenen scheiben, ZAMM 61 (1981) 105–106.
[13] J. Balas, J. Sladek and V. Sladek, Stress Analysis by Boundary Element Methods (Elsevier, Amsterdam, 1989).
[14] H. Hong and J. Chen, Derivatives of integral equations of elasticity, J. Engrg. Mech. 114(6) (1988) 1028–1044.
[15] A. Portela, M.H. Aliabadi and D.P. Rooke, The dual boundary element method: effective implementation for crack problems, Int. J. Numer. Methods Engrg. 33 (1992) 1269–1287.
[16] M.H. Aliabadi, The evaluation of the stress intensity factors using the two-dimensional boundary element method, Technical Report EMR/10/2, Engineering Materials Department, Southampton University, June 1985.
[17] M. Tanaka and H. Itoh, New crack elements for boundary element analysis of elastostatics considering arbitrary stress singularities, Appl. Math. Modell. 11 (1987) 357–363.
[18] T.A. Cruse and R.B. Wilson, Boundary integral equation method for elastic fracture mechanics analysis, Technical Report AFOSR-TR-780355, Pratt and Whitney Aircraft Group, 1977.
[19] M.D. Snyder and T.A. Cruse, Boundary integral equation analysis of cracked anisotropic plates, Int. J. Fracture 11 (1975) 315–328.
[20] T.A. Cruse, Boundary Element Analysis in Computational Fracture Mechanics (Kluwer Academic Publishers, Dordrecht, 1989).
[21] M.H. Aliabadi and D.P. Rooke, Numerical Fracture Mechanics (Computational Mechanics Publications and Kluwer, Southampton and Dordrecht, 1991).
[22] H. Rajiyah and S.N. Atluri, Evaluation of K-factors and weight functions for 2-D mixed-mode multiple cracks by the boundary element alternating method, Engrg. Fracture Mech. 32 (1989) 911–922.
[23] I.S. Raju and T. Krishnamurthy, A boundary element alternating method for two-dimensional mixed-mode fracture mechanics, Comput. Mech. 10 (1992) 133–150.
[24] C.W. Cheung, Y. K. and Woo and Y.H. Wang, A general method for multiple crack problems in a finite plate, Comput. Mech. 10 (1992) 335–343.
[25] Y.Z. Chen and N. Hasebe, An alternative Fedholm integral equation approach for multiple crack problem and multiple ridid line problem in plane elasticity, Engrg. Fracture Mech. 43(2) (1992) 257–268.
[26] K.Y. Lam and S.P. Phua, Multiple crack interaction and its effect on stress intensity factor, Engrg. Fracture Mech. 40(3) (1991) 585–592.
[27] F. Erdogan, G.D. Gupta and T.S. Cook, Numerical solution of singular integral equations, in: G.C. Sih, ed., Mechanics of Fracture 1: Methods of Analysis and Solutions of Crack Problems (Noordhoff, 1973) 368–425.
[28] P.S. Theocaris and N.I. Ioakimidis, Numerical integration method for the solution of singular integral equations, Quart. Appl. Math. 35 (1977) 173–183.
[29] V.V. Panasyuk, M.P. Savruk and A.P. Datsyshyn, A general method of solution of two-dimensional problems in the theory of cracks, Engrg. Fracture Mech. 9 (1977) 481–497.
[30] D.T. Barr and M.P. Cleary, Thermoelastic fracture solutions using distributions of singular influence functions—I: Determining crack stress fields from dislocation distributions, Int. J. Solids Struct. 19(1) (1983) 73–82.
[31] M. Denda, Complex variable Green's function representation of plane inelastic deformation in isotropic solids, Acta Mech. 72 (1988) 205–221.
[32] M. Denda, Formulation of the plastic source method for plane inelastic problems, Part 1: Green's functions for plane inelastic deformation. Acta Mech. 75 (1988) 93–109.
[33] M.A. Jaswon and G.T. Symm, Integral Equation Methods in Potential Theory and Elastostatics (Academic Press, London, 1977).
[34] M. Denda and Y.F. Dong, Explicit boundary element method formulas in complex variables, submitted for publication.
[35] G.M.L. Gladwell and A.H. England, Orthogonal polynomial solutions to some mixed boundary-value problems in elasticity theory, Q. J. Mech. Appl. Math. Pt. 2 (1977) 175–185.
[36] J.N. Dewynne, D.A. Hills and D. Nowell, Calculation of the opening dislacement of surface-breaking plane cracks, Comput. Methods Appl. Mech. Engrg. 97 (1992) 321–331.
[37] Y. Murakami et al. ed., Stress Intensity Factor Handbook (Pergamon Press, Oxford, 1987).